Eur. Phys. J. D **17**, 319–328 (2001)

THE EUROPEAN PHYSICAL JOURNAL D

EDP Sciences

Inversion analysis of K_2 coupled electronic states with the Fourier grid method

Ch. Lisdat[1], O. Dulieu[2,a], H. Knöckel[1], and E. Tiemann[1,b]

[1] Institut für Quantenoptik, Universität Hannover, Welfengarten 1, 30167 Hannover, Germany
[2] Laboratoire Aimé Cotton[c], CNRS, bâtiment 505, Campus d'Orsay, 91405 Orsay Cedex, France

Received 12 June 2001 and Received in final form 3 September 2001

Abstract. We present a new determination of the potential curves and interactions of the coupled electronic states $A\ ^1\Sigma_u^+$ and $b\ ^3\Pi_u$ of the potassium dimer, based on new laser spectroscopy measurements within a molecular beam, combined with data available in the literature. We used a new global deperturbation approach, involving the Fourier Grid Hamiltonian method for energy level calculation. A standard deviation of 1.2 is obtained corresponding to a variance of 7.5×10^{-3} cm^{-1}, representing a significant improvement compared to the standard deviation of 4 yielded by the traditional local deperturbation approach.

PACS. 32.80.Pj Optical cooling of atoms; trapping – 34.50.Rk Laser-modified scattering and reactions

1 Introduction

One major goal of molecular spectroscopy is the extraction of parameters describing the internal dynamics of molecules from measured transition energies. Due to their simplicity, diatomic molecules offer the possibility to test with a very high accuracy, inversion methods yielding potential energy and various spectroscopic constants. The traditional approach consists first in fitting observed transition energies to an analytical expression for energy levels involving vibrational and rotational quantum numbers, and second by an iterative calculation of the potential energy curve using the semi-classical Rydberg-Klein-Rees (RKR) method [1–4]. The RKR method is intrinsically limited to single-state single-well potential determination, and cannot deal with couplings of several states like in the breakdown of the Born-Oppenheimer approximation. In order to overcome these limitations, approaches based on direct fits of observed data to potential energy functions have been developed for atom-diatom van der Waals systems [5][1]. For diatomic molecules, it is known as the Inverted Perturbation Analysis (IPA) [6,7], and has been widely used to determine corrections to RKR potential curves. Among the most recent developments on the inversion of level energies to a potential, elaborated fully analytical potential functions have been employed to fit a large set of transition energies, even taking into account the long-range behaviour of the potential curve, varying as an inverse power law R^{-n} with the interatomic distance R (see [8], and references therein, and [9,10]).

However, all the above studies are dealing with single potential determinations. In the present work, we propose, for the first time to our knowledge, a direct generalization of the inversion procedure to the determination of several coupled potential curves, using a new flexible analytical function for potential representation [10], together with the recently developed mapped Fourier grid method (MFGH) [11] for eigenvalue computation. Indeed, it appeared during the analysis, that standard deperturbation methods based on an energy-localized modeling of level interactions [12], were not able to fully interpret the observed transitions. Let us mention that a first attempt to perform a coupled state analysis for the determination of the asymptotic potential has been proposed in a simplified way, for the treatment of cold-atom photoassociation spectra [13].

We study here the $A\ ^1\Sigma_u^+$ and $b\ ^3\Pi_u$ excited electronic states of the K_2 molecule, coupled by spin-orbit interaction (see Fig. 1). The motivation comes from our recent development of a molecular interferometer with K_2 molecules [14], involving the population of rovibrational levels of the long-lived $b\ ^3\Pi_u$ state, by perturbation facilitated excitation. This is a long-known example of singlet-triplet mixing in alkali dimers [15], which has been extensively studied in the past for the lightest species Li_2 [16–18], Na_2 [19,20], and K_2 [21–23], and more recently for Rb_2 [24]. The $A \sim b$ coupling in alkali dimers is also a textbook example of perturbations in molecular spectroscopy [12]. Due to near-degeneracy of energy levels

[a] e-mail: dulieu@lac.u-psud.fr
[b] e-mail: tiemann@iqo.uni-hannover.de
[c] UPR 3321 du CNRS

[1] In [5], the anisotropic part of the diatom-atom potential is taken as coupling potential yealding a system of coupled equations which then shows some physical similarity to the present problem.

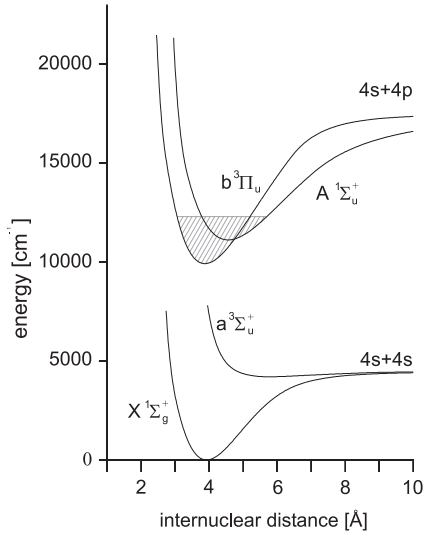

Fig. 1. Schematic view of the K_2 potential curves involved in the present study. The explored energy range is indicated as shaded area.

with same total angular momentum J, but belonging to different electronic states, the regularity of the spectrum (energy position or intensity of transition lines) is perturbed by their coupling. In contrast with the lightest species, the perturbation is so strong in the Rb_2 molecule that the entire regularity of the spectrum is apparently lost [24]. At the high level of spectroscopic accuracy, such a situation also occurs in K_2, which is successfully treated with the proposed coupled inversion method.

The paper is organized as follows: we recall in Section 2 the Hamiltonian describing the present system. The experimental set-up, using a molecular beam apparatus is briefly presented in Section 3 together with an example of recorded spectra, which is shown to complement previously published [22,23], and unpublished studies [25,26]. We give in Section 4 the results of our local deperturbation analysis. Our coupled inversion procedure is described in Section 5, resulting for the global deperturbation analysis of the spectra in improved potential curves for the A and b states of K_2, and accurate values for interaction terms.

2 Couplings between A $^1\Sigma_u^+$ and b $^3\Pi_u$ states

The Born-Oppenheimer states $A\ ^1\Sigma_u^+$ and $b\ ^3\Pi_u$, described in Hund's coupling case a, are assumed to interact mainly through spin-orbit and rotational coupling [12]. The spin-orbit coupling is represented in the deeply bound region of the potential as diagonal terms in the Hamiltonian and leads to the fine structure splitting of the 3 components of the b state, varying with the internuclear distance R:

$$\begin{aligned}\langle b\ \Omega=0|\mathbf{H}^{\rm SO}|b\ \Omega=0\rangle &= -A(R)\\ \langle b\ \Omega=1|\mathbf{H}^{\rm SO}|b\ \Omega=1\rangle &= 0\\ \langle b\ \Omega=2|\mathbf{H}^{\rm SO}|b\ \Omega=2\rangle &= +A(R). \end{aligned} \quad (1)$$

Ω is the projection of the total electronic angular momentum on the molecular axis. This description is not valid for the asymptotic part of the potential, that is not examined in this paper, but it is chosen for its simplicity and the direct comparability with previous analysis.

Additionally, the spin-orbit interaction leads to a non-diagonal matrix element $\zeta(R)$ coupling the $\Omega=0^+$ component of the b state with the A state:

$$\left\langle b\ ^3\Pi_u(0_u^+)\left|\mathbf{H}^{\rm SO}\right|A\ ^1\Sigma_u^+\right\rangle = \zeta(R). \quad (2)$$

A brief discussion on the asymptotic behaviour of equations (1, 2) and the connection of the atomic spin-orbit splitting of the $4p\ ^2$P to the parameter A will be given in Section 6. For states with total angular momentum J and projection Ω, the diagonal part of the rotational operator can be evaluated as [12]:

$$\begin{aligned}\left\langle JS\Omega\Sigma\left|\mathbf{H}^{\rm ROT}\right|JS\Omega\Sigma\right\rangle &= \frac{\hbar^2}{2\mu R^2}\\ &\times\left[J(J+1)-\Omega^2+S(S+1)-\Sigma^2\right] \end{aligned} \quad (3)$$

where S and Σ are respectively the total electron spin and its projection on the molecular axis, and μ the reduced mass of the system. The non-diagonal elements, referred to as spin-uncoupling terms [12] mix the different Ω components of the b state, giving in the present case:

$$\begin{aligned}\left\langle b\ JS\Sigma,\Omega\left|\mathbf{H}^{\rm ROT}\right|b\ JS\Sigma+1,\Omega+1\right\rangle &= \frac{\hbar^2}{2\mu R^2}\\ \times\sqrt{J(J+1)-\Omega(\Omega+1)}&\sqrt{S(S+1)-\Sigma(\Sigma+1)}. \end{aligned} \quad (4)$$

Other relativistic couplings might contribute significantly to the energy, although with much smaller magnitude than spin-orbit and rotational couplings. Among them, matrix elements of the spin-spin coupling $\mathbf{H}^{\rm SS}$ and the spin-rotational coupling $\mathbf{H}^{\rm SR}$ can be evaluated as follows [12]:

$$\begin{aligned}\left\langle JS\Lambda\Omega\left|\mathbf{H}^{\rm SS}\right|JS\Lambda\Omega\right\rangle &= \varepsilon[3\Sigma^2-S(S+1)]\\ \left\langle JS\Lambda\Omega\left|\mathbf{H}^{\rm SR}\right|JS\Lambda\Omega\right\rangle &= \gamma\left[\Sigma^2-S(S+1)\right]\\ \left\langle JS\Lambda\Omega\left|\mathbf{H}^{\rm SR}\right|JS\Lambda\Omega+1\right\rangle &= (\gamma/2)\\ \times\sqrt{J(J+1)-\Omega(\Omega+1)}&\sqrt{S(S+1)-\Sigma(\Sigma+1)} \end{aligned} \quad (5)$$

where ε and γ depend on R. These elements obviously vanish for the A state ($S=0$) but not for the b state ($S=1$). The influence of the spin-spin and spin-rotational coupling are expected to be small compared to the spin-orbit coupling. In the case of $\mathbf{H}^{\rm SR}$ the order of magnitude is given by $\gamma\propto(m_{\rm e}/m_{\rm n})\zeta$, where $m_{\rm e}$ and $m_{\rm n}$ are the electron and neutron mass, respectively [12]. With $\zeta\approx 19$ cm^{-1} for K_2 [22], one finds $\gamma\sim 0.01$ cm^{-1}. The rotational constant of the $b\ ^3\Pi_u$ state is approximately 0.057 cm^{-1} [22]. Therefore, the influence of γ can be of a significant magnitude, although small compared to A and ζ, which are both of comparable magnitude. Λ-doubling contribution is not considered in the present model, as it is not observed in the experimental spectra.

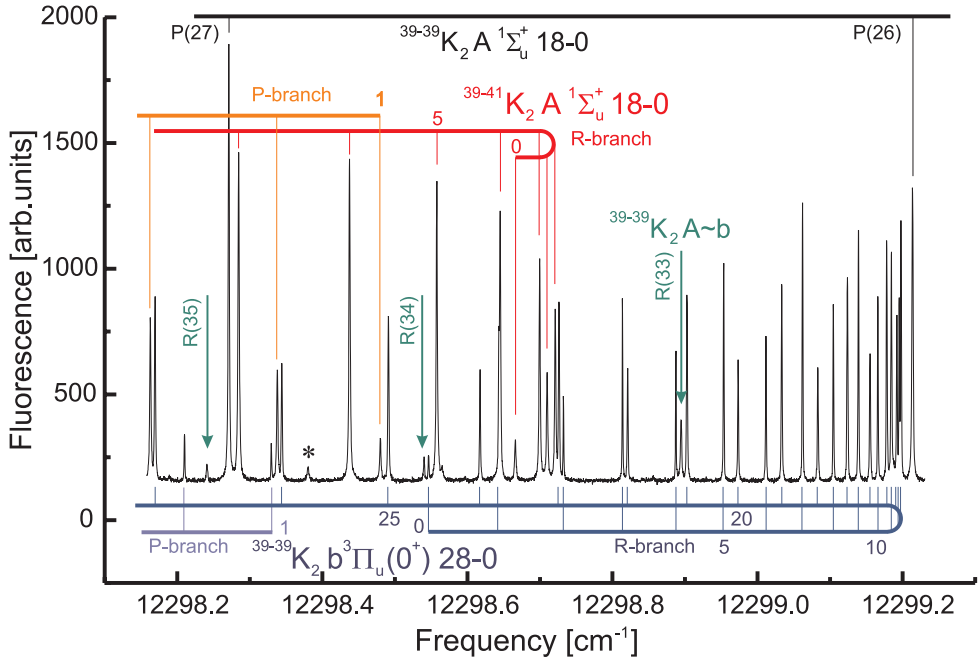

Fig. 2. Example of observed bands from transitions $b \leftarrow X$ in $^{39}K_2$ and $A \leftarrow X$ in $^{39-41}K_2$ (both with P- and R-branch). The few lines indicated by arrows are assigned to the R-branch of the coupled system $A(v = 18) \sim b(v = 28)$ based on the deperturbation analysis (compare Sect. 5). The R-branch dies out at those J'' values due to the thermal population, but from the P-branch, only $J'' = 26, 27$ are seen in this range. The $*$ symbol marks a remaining unassigned line.

The only influence of the spin-spin interaction is an unequal spacing of the fine structure components of the $b\,^3\Pi_u$ state, which will be observable only if detailed data are available for all components of the b state.

The $\mathbf{H}^{\mathrm{SO}}$ term in the Hamiltonian is the only one which mixes the singlet A state to the triplet b state. The diagonalization of the 4×4 total Hamiltonian for the coupling of the electronic states A and b, written in Hund's case a, for a given J, results in rovibrational levels, with more or less singlet and triplet character. Consequently, this induces a transition moment from the $X\,^1\Sigma_g^+$ ground state towards all levels of the coupled $(A \sim b)$ system. Even when the admixture of the singlet character is small, $X\,^1\Sigma_g^+ \rightarrow b\,^3\Pi_u(0_u^+)$ excitations should be observable with a sufficiently sensitive experimental set-up.

3 Experimental set-up and spectra for the (A ∼ b ← X) transitions

In our experiment we are using a molecular beam apparatus. The molecules are produced by evaporating potassium at 400 °C in an oven. The potassium vapor expands through a nozzle of 300 μm diameter, which is heated to about 430 °C to avoid clogging. The potassium dimers are predominantly produced in the $X\,^1\Sigma_g^+$ vibrational ground state ($v = 0$), since the potassium vapor undergoes a supersonic expansion, which cools the internal degrees of freedom of the molecule. The collimation ratio of the beam is approximately 1 000, which leads to a Doppler width of 1 MHz after excitation with light from a diode laser. K_2 molecules are detected by observing their total fluorescence with a red sensitive photomultiplier (Hamamatsu R 943-02). Excitation wavelengths were varied from 800 nm to 840 nm. The laser intensity required for a sufficient signal-to-noise ratio is below 10 mW. The frequency calibration is performed by a temperature stabilized marker cavity with a free spectral range of 150 MHz and the I_2 absorption spectrum [28]. The uncertainty of this calibration is estimated to 0.005 cm^{-1}. The fluorescence to be detected spreads from the excitation wavelength to roughly 1.2 μm. The tube is only sensitive up to ∼900 nm, which limited the low frequency part of the spectral detection window. To suppress laser stray light, we used a color glass (Schott RG 850 3 mm, cut-off $\lambda < 850$ nm) and an interference filter (center wavelength $\lambda = 878$ nm, FWHM = 51 nm). It was not possible to record spectra with excitation wavelength above 840 nm while having a reasonable suppression of laser stray light.

An example of a typical spectrum is given in Figure 2, showing among others a fully developed band of the state $^3\Pi_u(0_u^+)$. Actually similar observations were possible for several bands of the b state. The $b\,^3\Pi_u(0_u^+)$ hyperfine splitting present in these bands of the b state [29] is not resolved in this scan. It will be neglected in the following analysis, since the hyperfine structure leads to fairly symmetric line profiles and has no significant influence on the frequency of the transition. We observed vibrational levels of the A state from $v_A = 13$ to 22, and of the b state from $v_b = 24$ to 31. Rotational quantum numbers J' up to 35 were reached. The range of observations was limited to high vibrational levels v by the decreasing Franck-Condon factors for transitions with $v'' = 0$ in the ground state.

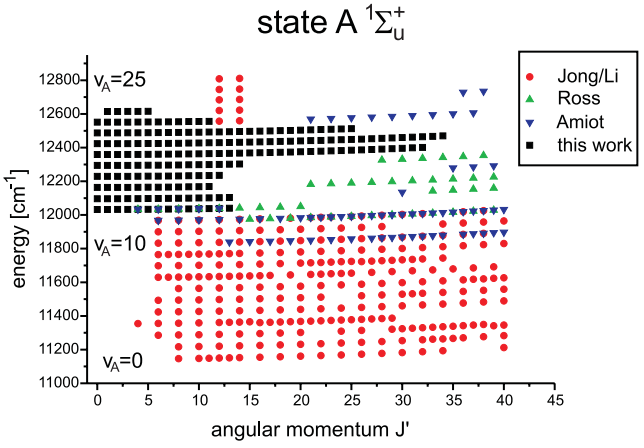

Fig. 3. Dataset of the $A\,^1\Sigma_u^+$ state used for the deperturbation analysis. Different authors are denoted by different symbols. The experimental uncertainties are 0.015 cm^{-1}, 0.04 cm^{-1} and 0.005 cm^{-1} for Jong *et al.* [22,25], Ross [30], and Amiot [26], respectively.

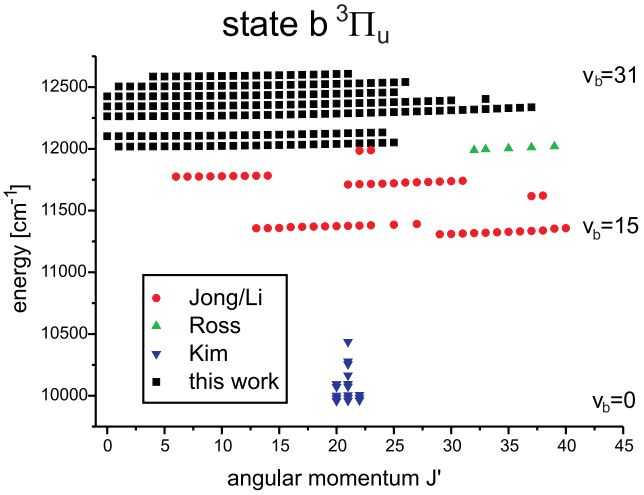

Fig. 4. Same as Figure 3 for the $b\,^3\Pi_u$ state. The experimental uncertainty for the term energies given by Kim [23] is 0.5 cm^{-1}.

To low v, we are limited by the sensitivity of our photomultiplier.

To our knowledge, these are the first observations of fully developed bands of $b\,^3\Pi_u - X\,^1\Sigma_g^+$ transitions in K_2. Actually, the present data are complementary to previous observations. An overview of the data available is shown in Figures 3 and 4. The present observations (squares in the figures) are spanning a range of vibrational levels unexplored up to now, with a rather dense set of J' values between 0 and 35 for both the A and b states. For the A state, published term energies already cover a rather dense grid. Levels in the range from $v_A = 0$ to 12 are available from Jong *et al.* [22]. Ross [30] and Amiot [26] provided us spectroscopic data for the A state measured by Fourier transform spectroscopy.

For the b state the situation is less favorable as only irregularly scattered term energies are known. Some term energies of perturbed levels of the b state were provided by Ross [30] and Li [25]. The latter were obtained under the experimental conditions described in [22]. The main part of the data belongs to the $\Omega = 0^+$ fine structure component, which has in general the largest singlet admixture and therefore is the component of the b state to be excited most easily from the $X\,^1\Sigma_g^+$ ground state. Only about 20 transitions to the $\Omega = 1, 2$ components are known presently. Therefore, the information about the fine structure splitting and the coupling constant A is limited. Additionally, nearly no term energies for levels below the minimum of the A state (see Fig. 1) are available besides the measurements given by Kim *et al.* in [23], which have large uncertainties of about 0.5 cm^{-1}.

All these data are put together to build up a comprehensive dataset, that we will use in the next sections for the deperturbation analysis. The data contain rotational quantum numbers J' below 40, except in the range $12 \leq v_A \leq 18$ for which transitions with rotational quantum numbers J' up to 100 are known [30]. For the triplet states no energies of such high J' levels are known, so a precise deperturbation in this region of quantum numbers is not possible. We restricted the dataset to $J < 40$ for the detailed analysis of the coupled states A and b, where the $\Omega = 0_u^+$ component will be the best determined component of the triplet manifold. However the location of the potential minimum of the b state will be affected by the large uncertainties of the data of reference [23].

4 Local deperturbation analysis of the spectra

Because rotational constants of different electronic states typically differ, rotational ladders of such states cross at a common J'. In the presence of a coupling between both ladders, the interaction increases with decreasing energetic spacing of levels with the same value of J', then repelling each other. This simplified picture has suggested a widely used approach to deperturb the spectra of coupled states (see for example Ref. [31]), based on the assumption that a vibrational level is perturbed by a limited set of neighbouring levels, and the influence of levels being further separated is neglected. The size of the subset remains limited to a few perturbing levels. Here we will report on a local deperturbation approach, which is described with some details below, in order to emphasize the differences with the global one, which is applied in the next section. The starting point is the equation of unperturbed rovibrational levels of an electronic state with given Ω using a Dunham-type expansion of term energies $E(v, J')$ [32]:

$$E_{J',v} = T_e + \sum_{l,k} Y_{lk}(v + 1/2)^l \left[J'(J' + 1) - \Omega^2\right]^k \quad (6)$$

where Y_{ij} are the usual Dunham parameters. The Hamiltonian operator for two rovibrational levels (J', v_A) and (J', v_b) coupled by spin-orbit and rotational interactions

$$\mathbf{H}_{\rm loc}(J', v_A, v_b) = \begin{array}{c} \begin{array}{cccc} A\,^1\Sigma_u^+ & b\,^3\Pi_{0_u^+} & b\,^3\Pi_{1_u} & b\,^3\Pi_{2_u} \end{array} \\ \begin{pmatrix} E_{J'v_A} & \zeta_0\langle v_A|v_b\rangle & 0 & 0 \\ \zeta_0\langle v_A|v_b\rangle & E_{J'v_b} + W_{00} - A_0 - \gamma + \varepsilon & \frac{\gamma}{2}\sqrt{2X} + W_{01} & W_{02} \\ 0 & \frac{\gamma}{2}\sqrt{2X} + W_{01} & E_{J'v_b} + W_{11} - 2(\gamma + \varepsilon) & \frac{\gamma}{2}\sqrt{2X-4} + W_{12} \\ 0 & W_{02} & \frac{\gamma}{2}\sqrt{2X-4} + W_{12} & E_{J'v_b} + W_{22} + A_0 - \gamma + \epsilon \end{pmatrix} \end{array} \quad (7)$$

(Eqs. (1–4)) leads to the following matrix structure:

see equation (7) above,

with $X = J'(J'+1)$. The spin-orbit functions A and ζ are assumed to be independent of R, therefore constants A_0 and ζ_0 appear, the latter multiplied by an overlap $\langle v_A|v_b\rangle$ between vibrational wavefunctions. The $W_{\Omega\Omega'}$ terms couple the components of the b state according to equation (4). The whole expression of the matrix elements has been already given in reference [31]. W_{02} appears through higher order centrifugal distortion. The contributions of spin-spin and spin-rotation terms (Eq. (5)) are also included.

The structure of the full Hamiltonian matrix used for the local deperturbation analysis is schematically drawn in Figure 5. The central diagonal block corresponds to the matrix in equation (7) for the pair of levels (J', v_A) and (J', v_b) under consideration, while the other diagonal blocks correspond to neighbouring pairs of interacting levels $(\tilde{v}_A, \tilde{v}_b)$. All diagonal blocks are interacting through off-diagonal elements (hashed area) connecting $\Omega = 0$ components. In the present work, we set up a matrix containing five (Fig. 5 shows only three) vibrational levels of the A and b states energetically centered around the considered level, leading to a 20×20 Hamiltonian matrix. A set of eight Dunham parameters for the electronic states is used, *i.e.* $k = 0, 1$ for $0 \le l \le 3$ in equation (6), giving the term energy ($k = 0$) and the rotational constant ($k = 1$) up to the third power in $(v + 1/2)$. In each iteration centrifugal distortion parameters were calculated based on the RKR potential following Hutson [33] and the energy levels corrected for centrifugal distortion effects for the next iteration step.

Twenty off-diagonal coupling elements are present to describe the local perturbation, all proportional to ζ_0 and to an overlap integral. Term energies are deduced from the diagonalization, and are transformed into transition energies using the Dunham parameters of the $X\ ^1\Sigma_g^+$ state [34].

By means of a non-linear fitting procedure [35], the Dunham parameters and coupling parameters are varied to reduce the sum $\chi^2 = \sum (E_{\rm obs} - E_{\rm cal})^2/\Delta^2$ of squared deviations between observed $E_{\rm obs}$ and calculated $E_{\rm cal}$ level energies, weighted by the square of the experimental uncertainties Δ. The overlap integrals $\langle v_A|v_b\rangle$, are calculated at each iteration from eigenfunctions in a RKR potential determined by the current values of Dunham parameters. These integrals depend only slightly on J'. Therefore, they are computed in steps of 20 rotational quanta, and a linear interpolation between them were found accurate enough.

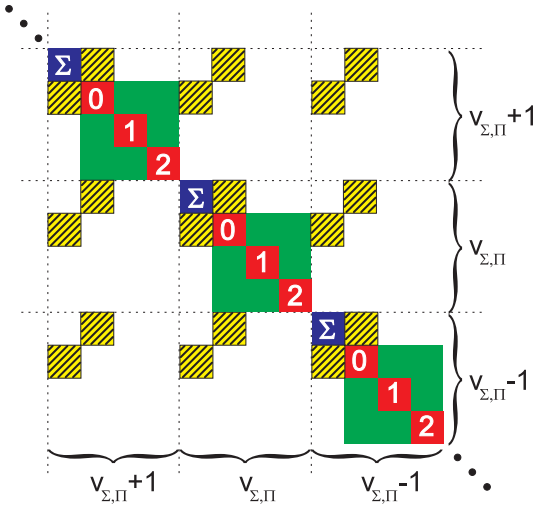

Fig. 5. Schematic representation of the Hamiltonian matrix to be diagonalized in the local deperturbation approach. Each diagonal block has the structure defined by equation (7). The labels 0, 1, and 2 hold for Ω values in the b state, and Σ for the A state. Off-diagonal hatched squares couple elements between different pairs of vibrational levels.

With this fitting algorithm, a description of the dataset with a σ (reduced chi-squared [36]) $\sigma = \sqrt{\chi^2/(N_{\rm obs} - N_{\rm par})} \approx 4$ was achieved. $N_{\rm obs}$ and $N_{\rm cal}$ are the numbers of observed transitions and adjusted parameters, respectively. The deviations of the lowest vibrational levels of the A state are mainly responsible for the large σ. For example, the rotational levels of $v_A = 0$ calculated by the fitting program remained shifted systematically by about 0.1 $\rm cm^{-1}$ to lower energies with respect to the observed ones. Excluding $v_A = 0$ from the fit improved the fit to $\sigma \approx 2.6$. Neither a larger number of Dunham parameters, nor the introduction of R-variation of the non-diagonal spin-orbit coupling (R-centroids expansion):

$$\left\langle b\,^3\Pi_u(0^+) \left| \mathbf{H}^{\rm SO} \right| A\,^1\Sigma_u^+ \right\rangle = \zeta\langle v_a|v_b\rangle + \xi\langle v_a|R|v_b\rangle \quad (8)$$

or v-dependent variations of the spin-orbit couplings according to:

$$\left\langle b\ \Omega = 0, 2 \left| \mathbf{H}^{\rm SO} \right| b\ \Omega = 0, 2 \right\rangle = \mp A \mp \alpha(v + 1/2) \quad (9)$$

improved the fitting results significantly. The R-centroids were calculated with the same RKR procedure used to calculate the overlap integrals. The unsatisfactory description of the potential minimum of the A state is surprising, because a power expansion like the Dunham series should

$$\mathbf{H} = \begin{array}{c} \begin{array}{cccc} A\,^1\Sigma_u^+ & b\,^3\Pi_{0_u^+} & b\,^3\Pi_{1_u} & b\,^3\Pi_{2_u} \end{array} \\ \begin{pmatrix} T_0^\Sigma + V_0^\Sigma + w_0^\Sigma & w_{00}^{\Sigma\Pi} & 0 & 0 \\ w_{00}^{\Sigma\Pi} & T_0^\Pi + V_0^\Pi + w_0^\Pi & w_{01}^{\Pi\Pi} & 0 \\ 0 & w_{01}^{\Pi\Pi} & T_1^\Pi + V_1^\Pi + w_1^\Pi & w_{12}^{\Pi\Pi} \\ 0 & 0 & w_{12}^{\Pi\Pi} & T_2^\Pi + V_2^\Pi + w_2^\Pi \end{pmatrix} \end{array} \tag{11}$$

be well adapted to this part of the potential, where the anharmonicity is low. It will turn out in the next section, that the limited dimension of the interaction matrix is the main reason for this failure. This prevents any influence of energetically far lying levels, which are in the present case the lowest triplet levels. The potential minimum of the A state is more sensitive to such effects than the other parts of the potential, due to the many b levels lying below, whereas in other regions this effect averages out due to perturbing levels below as well as above the studied one.

5 Global deperturbation

The failure of the present local deperturbation approach means, that an extension is needed where matrices significantly larger than 20×20 have to be diagonalized for each observed level at each fit iteration. Besides the quality of the fit, there is no obvious criterion where to truncate the number of perturbing levels. An alternative procedure consists, at each iteration step, in solving the set of four coupled Schrödinger equations in order to extract the whole eigenvalue spectrum of the coupled system. In this approach interactions among all vibrational levels are taken into account simultaneously. We choose the Fourier Grid Hamiltonian (FGH) method [37], which has proven to be well adapted to this kind of calculations [38,39].

A detailed presentation of the FGH method can be found for instance in [11], and we recall here only its main aspects. The total Hamiltonian $\mathbf{H} = \mathbf{T} + \mathbf{V}$ for a single electronic state with potential energy operator $\mathbf{V}$ and kinetic energy operator $\mathbf{T}$, is represented on a grid of length L with N equidistant points in R coordinate, leading to the matrix elements [38]:

$$\begin{aligned} V_{ij} &= V(R_i)\delta(i-j) \\ T_{ii} &= \frac{\pi^2}{\mu L^2}\frac{N^2+2}{6} \\ T_{ij} &= (-1)^{i-j}\frac{\pi^2}{\mu L^2}\frac{1}{\sin^2[(i-j)\pi/N]}. \end{aligned} \tag{10}$$

Such a $N \times N$ matrix representation is equivalent to the choice of a basis of N plane wavefunctions in the momentum space, with N discrete values of momentum. For p interacting states, the Hamiltonian matrix has a $(pN) \times (pN)$ dimension, and is structured for the present case ($p = 4$) as:

see equation (11) above,

where the indices of the elements are related to the Ω values. In this expression, elements T_Ω and V_Ω are $N \times N$ submatrices defined by equation (10). The $N \times N$ diagonal blocks $w_{\Omega\Omega'}$ contain matrix elements coupling the 4 electronic states, and are deduced from equations (2, 4) and the nondiagonal part of equation (5), while w_Ω blocks contains the diagonal parts of equations (1, 3, 5). It is noteworthy, that the matrix elements W_{ij} in equation (7) are averages over the internuclear distance R by the vibrational motion, while w_Ω is built up from the explicit values for given R.

Such a matrix is diagonalized, and provides eigenenergies and eigenfunctions for rovibrational levels of the coupled systems. When the coupling between a group of levels is efficient, the corresponding vibrational wavefunctions will have a complicated structure, resulting from the superposition of wavefunctions from the individual levels. Example of such wavefunctions can be found in references [38,39].

Matrix elements in equation (11) can be rearranged, in order to bring together matrix elements from blocks related to the same couple (i, j) of grid points. This provides the schematic picture of the structure of the potential energy matrix, displayed in Figure 6 for a few (i, j) pairs, giving the coupling between the electronic states at such pairs. The similarity with the local matrix of Figure 5 is obvious, except that there is no direct coupling between $\Omega = 0$ and $\Omega = 2$ components of the b state. This scheme shows that the representation of the Hamiltonian is now achieved on a complete basis set, instead of being limited to a small subset of vibrational wavefunctions. As visible in equation (10), the kinetic energy matrix is non-local, and has not a simple structure as the one shown in Figure 5.

In order to check the influence of the perturbations between distant A and b levels, we performed a diagonalization of the $\mathbf{H}$ matrix in equation (11) for $J = 0$ (*i.e.* a two-coupled state calculation, with $\Omega = 0$), using the RKR potentials and the interaction parameters determined in the local approach. The grid applied in the FGH method is chosen according to the maximum momentum to be represented in the calculation, deduced from the hashed zone in Figure 1. A number of equidistant points $N < 120$ covering the range of internuclear distances 3.5 a.u. $< R <$ 13.5 a.u. is sufficient. Only the 160 lowest eigenvalues of the $A \sim b$ mixed system are calculated, in order to shorten the computing time for the diagonalization. In Figure 7, the singlet component of the coupled system eigenvectors for $J' = 0$ is represented for levels located in the bottom of the b potential, up to the bottom

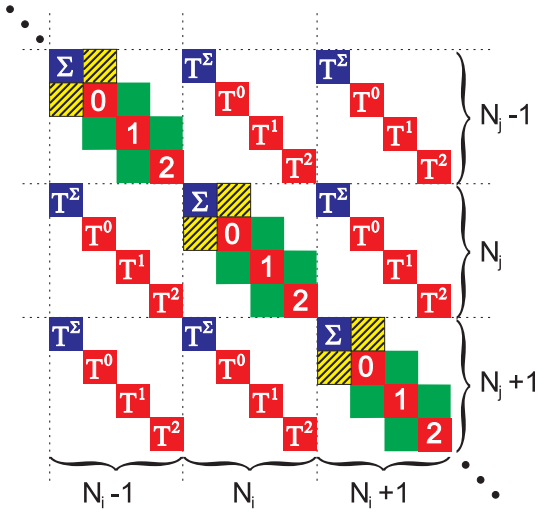

Fig. 6. Schematic representation of the $4N \times 4N$ Hamiltonian matrix to be diagonalized in the global deperturbation approach for the present $A \sim b$ system. Only three blocks corresponding to three arbitrary grid points $N_j, N_j \pm 1$, $(2 < N_j < N - 1)$ are represented here for illustration. The labels 0, 1, and 2 hold for Ω values in the b state, and Σ for the A state. Diagonal matrix elements Σ, 0, 1, and 2 contain contributions from both kinetic and potential energy. Off-diagonal contributions of the kinetic energy are denoted by T^{Σ}, T^0, T^1, T^2. Remaining pictured areas without symbols are elements coupling the 4 electronic states (Eqs. (2, 4, 5)).

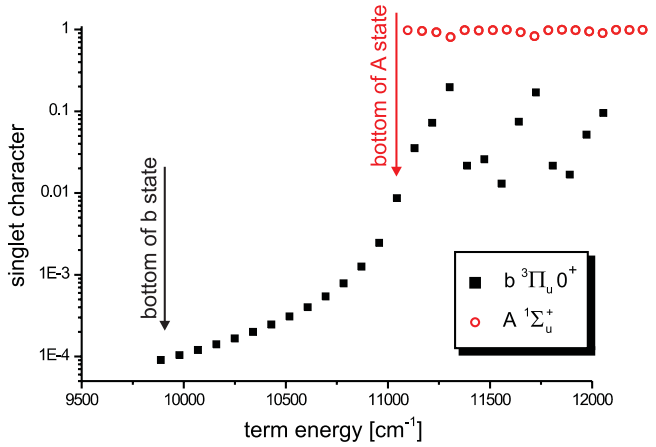

Fig. 7. Singlet component of eigenvectors of the $A \sim b$ coupled states in K_2. A and b labeling is assigned when this component is respectively larger or lower than 1/2.

of the A potential. Strong and localized perturbations are visible for 2 levels (around 11 300 and 11 700 cm^{-1}), when the triplet contribution to the singlet component increases abruptly and the reverse happens for the triplet component. But, it is worth noticing that levels located below the bottom of the A state have a non-negligible ($\approx 10^{-4}$) singlet character. Even more striking is the energy shift of these levels induced by the coupling with all other A levels, when compared to their energy deduced from a diagonalization where the coupling term w_{00} is put to zero.

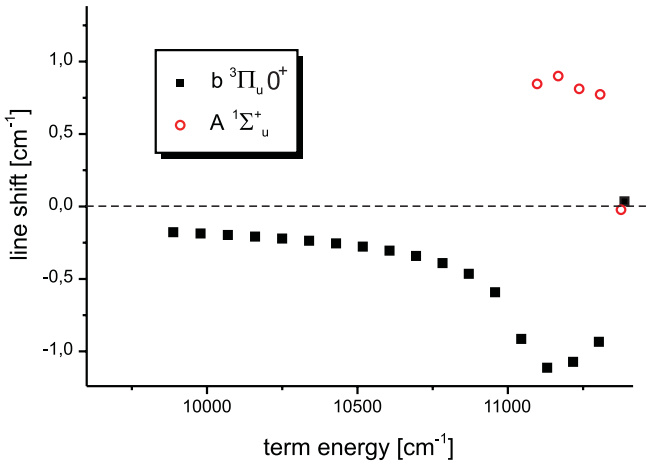

Fig. 8. Computed energy shift of the lowest b levels induced by the coupling, when compared to their energy computed for vanishing coupling.

Figure 8 shows that a shift of 0.2 cm^{-1} is predicted for the $v_b = 0$ level of the b state. This preliminary calculation confirms that a global analysis of the perturbations is necessary, as all levels are interacting together.

To adjust the potential curves for fitting the experimental data, we chose an analytical expression for the potential curves V_0^{Σ} and $V_{0,1,2}^{\Pi}$ in equation (11). The analytical form is divided into three parts, connected at the internuclear distances R_i and R_o $(R_i < R_o)$. The middle part from R_i to R_o around the potential minimum roughly at R_m is given by the series [10]:

$$V(R) = \sum_i a_i \left(\frac{R - R_m}{R + bR_m} \right)^i, \quad i \geq 0. \qquad (12)$$

b is a convergence improving factor fixed for each potential curve. The coefficients a_i determine the shape of the potential and are adjustable by a fitting procedure comparable to the one described in Section 4. The internuclear distance R_{min} at the potential minimum can be calculated from equation (12), values for the final set of parameters a_i are given in Table 1.

The same coefficients a_i were used for all fine structure components of the b state. The values of $R_{i,o}$ were chosen such that the potential energy $V(R_{i,o})$ is slightly higher than the largest term energy included in the data set. Therefore, the part of the potential curve for which spectroscopic information is included in the fit, is completely determined by equation (12). Inner and outer part only ensure a correct behaviour of the wave function in the classical forbidden region, and should not be used for further spectroscopic predictions outside the range studied here.

For internuclear distances $R < R_i$, the repulsive inner part of the potential was described by the expression

$$V_i(R) = A_i e^{-B_i(R - R_i)} \quad \text{for } R < R_i. \qquad (13)$$

Parameters A_i and B_i were chosen to make the potential continuous at $R = R_i$, as well as its first derivative.

Table 1. Values of parameters for the $A\,^1\Sigma_u^+$ and $b\,^3\Pi_u$ states of K_2, and their interaction. R_m, R_i, R_o, and b are kept during the fitting procedure. Parameters a_0 to a_9, A, ζ_0, and ζ_2 are provided by the global fitting procedure. Values for the location of potential minimum R_{min}, the crossing point R_{Ab}, and the energy difference between potential minimum Δ_{Ab} for the A and b states, deduced from the fitted curves, are also displayed, and compared to previous determinations. Estimated standard deviations are given in parenthesis.

$A\,^1\Sigma_u^+$		$b\,^3\Pi_u$	
R_m	4.55078 Å	R_m	3.89453 Å
R_i	3.55 Å	R_i	2.95 Å
R_o	6.55 Å	R_o	6.50 Å
b	0.27	b	−0.28
a_0	11 107.1405 cm^{-1}	a_0	9 912.9473 cm^{-1}
a_1	0.10074654×10^3 cm^{-1}	a_1	0.50271825×10^3 cm^{-1}
a_2	0.48011869×10^5 cm^{-1}	a_2	0.18377386×10^5 cm^{-1}
a_3	-0.3013653×10^5 cm^{-1}	a_3	0.7978306×10^4 cm^{-1}
a_4	-0.253938×10^5 cm^{-1}	a_4	0.747073×10^4 cm^{-1}
a_5	0.160462×10^6 cm^{-1}	a_5	0.377933×10^5 cm^{-1}
a_6	-0.640140×10^6 cm^{-1}	a_6	-0.293825×10^5 cm^{-1}
a_7	0.118110×10^6 cm^{-1}	a_7	-0.166277×10^6 cm^{-1}
a_8	0.224542×10^7 cm^{-1}	a_8	-0.972435×10^5 cm^{-1}
		a_9	0.10070×10^7 cm^{-1}
		A	21.3145(80) cm^{-1}
			(21.75(8) cm^{-1} [22])
ζ_0	18.3021(50) cm^{-1} (18.64(9) cm^{-1} [22])		
R_{SO}	4.681965(40) Å		
ζ_2	33.635(10) cm^{-1}Å^{-2}		
R^{Σ}_{min}	4.5447 Å	R^{Π}_{min}	3.8564 Å
R_{Ab}	4.755 Å		
	4.735 Å [44]		
Δ_{Ab}	1 197.7(1) (5)* cm^{-1}		
	1 196.1(18) cm^{-1} [22]		
	1 198.8(1) cm^{-1} [23]		
	1 185 cm^{-1} [44]		

* Error from data in [23].

For the long-range part of the potential with $R > R_o$ the asymptotic form

$$V_o(R) = D - \frac{C_3}{R^3} - \frac{C_6}{R^6} + E_{ex}(R) \quad \text{for } R > R_o$$
$$E_{ex}(R) = -A_{ex}e^{-B_{ex}R} \tag{14}$$

was used. Values for asymptotic coefficients, C_3 and C_6 were taken from [40], while A_{ex} and B_{ex} were used to connect the middle and outer part of the potential in a continuous and differentiable way. D is the energy of the dissociation limit, calculated here from the dissociation energy of the ground state [41] and the transition frequencies of the atomic D_1 and D_2 lines [42]. It is important to notice that parameters C_3, C_6, D, A_{ex}, B_{ex}, A_i, and B_i are not fitting parameters. Their values are reported in the Appendix.

In addition to the coefficients a_i in equation (12), the coupling matrix elements in equation (11) were varied by the fitting program using the same package [35] as for the local fit. Fits with 9 and 10 parameters a_i for the A and b state, respectively, and two spin-orbit parameters A and ζ (Eqs. (1, 2), independent of R) improved the description of the experimental results significantly to $\sigma \approx 1.8$. This is a strong support for the need of a global approach, since the local deperturbation one reached only $\sigma \approx 4$ with a comparable number of Dunham parameters and the same couplings between the four electronic components as it was discussed in Section 4. Especially, the significant deviations for the lowest vibrational levels in the A state are drastically reduced, which is in our opinion due to the influence of the lower levels of the triplet state, which are taken into account in this approach now.

In extended fits the spin-rotational coupling (Eq. (5)) was introduced, which leads to a further improvement ($\sigma \approx 1.4$). The ratio of the fitted parameters ζ and γ was in very good agreement with the expected value as discussed in Section 2. The spin-spin coupling was neglected, since only very few term energies of the $\Omega = 1, 2$ components of the b state are contained in the dataset, which results in very limited knowledge of the energetic separation of the three potential curves.

In a third fit a R-dependence of the spin-orbit interactions (Eqs. (1, 2)) was allowed instead of the spin-rotational coupling. Based on the results of *ab initio* calculations by Meyer for Na_2 [43], the variations of the constants A and ζ with R were approximated in the explored range of R by parabolas with their minimum at R_{SO} near the crossing point of A and b state. Only the dependence of ζ on the internuclear distance turned out to be significant and was described by:

$$\zeta(R) = \zeta_0 + \zeta_2(R - R_{SO})^2. \tag{15}$$

All three parameters ζ_0, ζ_2, and R_{SO} were adjusted by the fit. The σ of the fit reached a value below 1.2, which corresponds to a variance $s = \sqrt{N_{obs}\sigma^2/\sum \Delta^{-2}}$ [36] of 7.5×10^{-3} cm^{-1}. The description of the experimental data did not improve further by additional spin-rotational coupling. Spin-rotational coupling and variation of ζ with R probably cannot be separated, since too few data are available for the $\Omega = 1, 2$ components of the b state. The range of internuclear distance R, where the derived R-dependence of ζ is applicable, is much smaller than the R-range of the determined potentials, since the influence of $\zeta(R)$ is restricted to regions of non-vanishing overlap between the wavefunctions in both potentials.

The obtained parameters of this last fit are given in Table 1. This set of parameters reproduces the experimental data in the best way of all fits and, on average, essentially within the estimated experimental uncertainties. Furthermore, transition frequencies could be predicted in the vicinity of observed transitions, that allowed the assignment of yet unidentified transitions with

deviations between observed and measured frequencies below 0.005 cm^{-1} (*e.g.* Fig. 2, indicated by arrows).

6 Discussion

In this paper we have described two fundamentally different approaches for the deperturbation of spectra of diatomic molecules on the example of the K_2 molecule to derive a set of parameters by non-linear fitting, that will reproduce the experimental data. The first discussed local deperturbation (Sect. 4) uses Dunham-type parameters to describe the energies of the molecular levels and takes into account the interaction between a limited number of perturbing levels only. This approach did not lead to a satisfying fit.

By the utilization of a potential fit and the FGH method to calculate the eigenvalues of the coupled system in the basis of electronic states, the results of the fit improved significantly. This is especially remarkable, because no new couplings compared to the local approach were considered, but only the yet neglected perturbations by energetically far lying levels were taken into account. For the levels in the minimum of the b state we have shown, that perturbations can sum up to energy shifts, which are many times larger than the experimental accuracy of typical laser spectroscopy experiments (Fig. 8). Therefore, we think the large difference in the results of both approaches must be attributed to non-local couplings. Additionally, this shows the necessity of a global deperturbation analysis even for moderately perturbed systems, when the experimental accuracy is high.

The FGH allows easily the implementation of different, especially R-dependent interactions between the electronic states. With this degree of freedom for the spin-orbit coupling between A and b state (Eqs. (2, 15)) it was possible to improve the fit further, nearly to a description of the experimental data within their uncertainties, *i.e.* a σ of 1.2.

The spin-orbit coupling parameters (Eqs. (1, 2)) obtained from the fit can be compared with the atomic spin-orbit splitting Δ for the $4p$ state of the potassium atom. From the theory of long-range interaction (*e.g.* [40]) one finds $\sqrt{2}\Delta/3$ for the magnitude of the spin-orbit coupling between two $\Omega = 0$ components of A and b states. This asymptotic value corresponds to ζ_0 used here in equation (2). With $\Delta = 57.6848(1)$ cm^{-1} [42] the long range theory predicts $\zeta \approx 27.2$ cm^{-1} at large R. The determined coupling function with ζ_0 and ζ_2 parameters cannot be used for a direct comparison, because it has not the appropriate asymptotic behaviour. But the sign of ζ_2 indicates that ζ increases for large R, starting from ζ_0 =18.3 cm^{-1} at 4.68 Å.

For the comparison of the molecular fine structure splitting A (Eq. (1)) with the atomic value Δ the best is to compare the splitting between the $\Omega = 0_u^+$ and 2_u component of the b state, since both subspaces of electronic states at a $s+p$ asymptote are fully included in the deperturbation analysis, while the $\Omega = 1_u$ space (in total three dimensional for the $s + p$ asymptote) is truncated to one state. The asymptotic formulas (compare [40]) predict for the inner part of the potential a splitting of $2\Delta/3 \approx 38.5$ cm^{-1}, which is in good agreement with the value of $2A \approx 42.6$ cm^{-1} in Table 1. Therefore, the R dependence of A seems to be weak, which was also indicated by the low significance of a function $A(R)$ instead of $A = const$ in the fit (Sect. 5).

The present determinations of interaction parameters yields a difference of 1.7% with previous experimental values reported by Jong *et al.* [22]. Such an agreement is satisfactory, keeping in mind that the value of reference [22] is obtained after averaging over all vibrational levels studied with a local deperturbation approach, while in the present work, interaction parameters are extracted from a single analysis of all concerned vibrational levels. Furthermore, the agreement of the pseudopotential calculations of reference [44] with the present potential curves is good, as illustrated by the location of the crossing point R_{Ab} between the A and b states, and by the energy difference Δ_{Ab} of the bottom of their well.

In a next step, already known data [26] of higher vibrational levels of the A state will be included to extend the potential to larger internuclear distances. Since the experimental knowledge of the b state is rather poor for higher energies, this analysis will probably be restricted to a one channel calculation for the $^1\Sigma_u^+$ state only. Experiments to obtain data within the existing gap to the asymptotic levels measured by photoassociation spectroscopy [40] and to perform a vibrational assignment of those levels are in progress in our group. They will use a Franck-Condon pumping scheme as applied successfully in experiments with Na_2 [45] to reach asymptotic states of the well bound molecule.

The non-negligible mixing of $A\ ^1\Sigma_u^+$ and $b\ ^3\Pi_u$ states predicted for levels below the minimum of the A state (Fig. 7) can be of experimental interest, since it generates an electric dipole transition moment to the $X\ ^1\Sigma_g^+$ ground state. In principle, the spectroscopic analysis of this part of the b state potential with a single laser excitation should be possible. Those weak transitions to a long-lived electronically excited state can also be used for matter wave interferometry with higher resolution compared to our present results [14].

The authors thank A. Ross, C. Amiot, and L. Li for kindly providing us unpublished spectroscopic data for the analysis. Critical reading of the manuscript by C. Amiot is also gratefully acknowledged. This work was supported by the Deutsche Forschungsgemeinschaft within the SFB 407, and by the joint CNRS/DAAD Procope program.

Appendix

We report for completeness in Table 2, the values for parameters describing the potential curves outside the range of the present spectroscopic study. Whereas values for C_3,

Table 2. Parameters used in the present analysis, for the representation of the potential curves outside the $[R_i, R_o]$ interval.

	A state	b state
C_3 [40]	16.872 a.u.	8.436 a.u.
C_6 [40]	9 365 a.u.	6 272 a.u.
D [41,42]	17 435.860(75) cm^{-1}	17 493.570(75) cm^{-1}
A_{ex}	0.2401114×10^4 cm^{-1}	0.8793316×10^4 cm^{-1}
B_{ex}	0.3950582 $Å^{-1}$	0.6137710 $Å^{-1}$
A_i	0.133073137×10^5 cm^{-1}	0.130439338×10^5 cm^{-1}
B_i	0.38414294 $Å^{-1}$	0.63223242 $Å^{-1}$

C_6, and D are taken from the literature, values for A_{ex}, B_{ex}, A_i, and B_i are reevaluated after each iteration, to ensure continuity of the potential functions during the whole fitting process. These parameters cannot be used for any spectroscopic prediction.

References

1. R. Rydberg, Z. Phys. **73**, 376 (1931).
2. O. Klein, Z. Phys. **76**, 226 (1932).
3. R. Rydberg, Z. Phys. **80**, 514 (1933).
4. A.L.G. Rees, Proc. Phys. Soc. (London) **59**, 998 (1947).
5. R.J. Le Roy, J. van Kranendonk, J. Chem. Phys. **61**, 4750 (1974).
6. W.M. Kosman, J. Hinze, J. Mol. Spectrosc. **56**, 93 (1975).
7. C.R. Vidal, H. Scheingraber, J. Mol. Spectrosc. **65**, 46 (1977).
8. P.G. Hajigeorgiou, R.J. Le Roy, J. Chem. Phys. **112**, 3949 (2000).
9. J.Y. Seto, R.J. Le Roy, J. Vergès, C. Amiot, J. Chem. Phys. **113**, 3067 (2000).
10. C. Samuelis, E. Tiesinga, T. Laue, M. Elbs, H. Knöckel, E. Tiemann, Phys. Rev. A **63**, 012710 (2000).
11. V. Kokoouline, O. Dulieu, R. Kosloff, F. Masnou-Seeuws, J. Chem. Phys. **110**, 9865 (1999).
12. H. Lefebvre-Brion, R.W. Field, *Perturbations in the spectra of diatomic molecules* (Academic Press, Inc., US, 1986).
13. J.M. Vogels, R.S. Freeland, C.C. Tsai, B.J. Verhaar, D.J. Heinzen, Phys. Rev. A **61**, 043407 (2000).
14. C. Lisdat, M. Frank, H. Knöckel, M.-L. Almazor, E. Tiemann, Eur. Phys. J. D **12**, 235 (2000).
15. R.W. Wood, F.E. Hackett, Astrophys. J. **30**, 339 (1909).
16. P. Kusch, M.M. Hessel, J. Chem. Phys. **67**, 586 (1977).
17. C. Linton, F. Martin, I. Russier, A.J. Ross, P. Crozet, S. Chinasy, R. Bacis, J. Mol. Spectrosc. **175**, 340 (1996).
18. K. Urbanski, S. Antonova, A.M. Lyyra, A. Yiannopoulou, W.C. Stwalley, J. Chem. Phys. **104**, 2813 (1996).
19. W.T. Luh, V. Zafiropoulos, P.D. Kleiber, W.C. Stwalley, S.P. Heneghan, J. Mol. Spectrosc. **111**, 327 (1985).
20. H.G. Krämer, M. Keil, J. Wang, R.A. Bernheim, W. Demtröder, Chem. Phys. Lett. **272**, 391 (1997).
21. A.M. Lyyra, W.-T. Luh, Li Li, H. Wang, W.C. Stwalley, J. Chem. Phys. **92**, 43 (1990).
22. G. Jong, L. Li, T.J. Whang, W.C. Stwalley, J.A. Coxon, M. Li, A.M. Lyyra, J. Mol. Spectrosc. **155**, 115 (1992).
23. J.T. Kim, H. Wang, C.C. Tsai, J.T. Bahns, W.C. Stwalley, G. Jong, A.M. Lyyra, J. Chem. Phys. **102**, 6646 (1995).
24. C. Amiot, O. Dulieu, J. Vergès, Phys. Rev. Lett. **83**, 2316 (1999).
25. Li Li, private communication.
26. C. Amiot, private communication.
27. A. Ross, P. Crozet, C. Effantin, J. D'Incan, R.F. Barrow, J. Phys. B **20**, 6225 (1987).
28. S. Gerstenkorn, J. Vergès, J. Chevillard, *Atlas du spectre d'absorption de la molécule d'iode [11 000-14 000 cm^{-1}]* (Laboratoire Aimé Cotton, CNRS II, Orsay, France, 1982).
29. C. Lisdat, H. Knöckel, E. Tiemann, J. Molec. Spect. **63**, 81 (2000).
30. A. Ross, private communication.
31. C. Effantin, O. Babaky, K. Hussein, J. D'Incan, R.F. Barrow, J. Phys. B **18**, 4077 (1985).
32. J.L. Dunham, Phys. Rev. **41**, 721 (1932).
33. J.M. Hutson, J. Phys. B **14**, 851 (1981). The program CDIST has been kindly provided by its author.
34. C. Amiot, J. Vergès, C.E. Fellows, J. Chem. Phys. **103**, 3350 (1995).
35. F. James, M. Roos, *MINUIT D506, CERN Program Library* (CERN, Geneva, 1989), Vol. D.
36. P.R. Bevington, D.K. Robinson, *Data reduction and error analysis for the physical sciences*, 2nd edn. (WCB/McGraw-Hill, US, 1992).
37. R. Kosloff, J. Phys. Chem. **92**, 2087 (1988).
38. O. Dulieu, P.S. Julienne, J. Chem. Phys. **103**, 60 (1995).
39. C. Amiot, O. Dulieu, J. Vergès, Phys. Rev. Lett. **83**, 2316 (1999).
40. H. Wang, P.L. Gould, W.C. Stwalley, J. Chem. Phys. **106**, 7899 (1997).
41. G. Zhao, W.T. Zemke, J.T. Kim, B. Ji, H. Wang, J.T. Bahns, W.C. Stwalley, Li Li, A.M. Lyyra, C. Amiot, J. Chem. Phys. **105**, 7976 (1996).
42. W. Scherf, O. Khait, H. Jäger, L. Windholz, Z. Phys. D **36**, 31 (1996).
43. W. Meyer, private communication.
44. S. Magnier, P. Millié, Phys. Rev. A **54**, 204 (1996).
45. M. Elbs, O. Keck, H. Knöckel, E. Tiemann, Z. Phys. D **42**, 49 (1997).